AIAA JOURNAL
Vol. 45, No. 3, March 2007

Crack-Induced Effects on Aeroelasticity of an Unswept Composite Wing

Kaihong Wang* and Daniel J. Inman†
Virginia Polytechnic Institute and State University, Blacksburg, Virginia 24060-0261

DOI: 10.2514/1.21689

Crack-induced changes in the aeroelastic boundaries of an unswept composite wing are investigated. The bending-torsion couplings due to the unbalanced laminates and offset of the center of gravity are incorporated into the equation of motion. The edge crack, modeled with the local flexibility concept, introduces additional boundary conditions at the crack location. The fundamental modes of the intact and cracked beam are used in Galerkin's method, and the approximate solution for flutter and divergence speeds is obtained with steady and quasi-steady aerodynamic forces applied. Changes in flutter and divergence speeds (with respect to the crack ratio and its location, along with the fiber orientation) are compared. In many cases, the existence of an edge crack imposes detrimental effects on the aeroelastic boundaries, although it may increase the flutter and/or divergence speed when fibers are orientated at certain angles. The results may help composite wing designers in their aeroelastic tailoring and structural engineers in designing damage prognosis tools to predict the health status of composite wing structures.

Nomenclature

a	=	crack width
b	=	beam width
C_L	=	lifting coefficient
c	=	beam thickness
EI	=	bending stiffness parameter
GJ	=	torsional stiffness parameter
$H(\xi)$	=	transverse displacement
$h(y, t)$	=	transverse displacement of the reference axis
I_{cg}	=	polar mass moment of inertia per unit length about the center of gravity
K	=	bending-torsion coupling parameter
L	=	lifting force, positive upward
l	=	beam length
l_c	=	crack location
M	=	pitching moment, positive nose up
$M(\xi)$	=	bending moment
m	=	mass per unit length
S_{cg}	=	offset of the center of gravity
$S(\xi)$	=	shear force
$T(\xi)$	=	torsional moment
U	=	speed of an incompressible air fluid
x_o	=	reference axis location
$\Theta(\xi)$	=	cross-sectional rotation
θ	=	fiber angle
λ	=	nonzero constant
$\Phi(\xi)$	=	twisting angle
$\phi(y, t)$	=	twisting angle of the reference axis

Introduction

FIBER-REINFORCED composite materials have been increasingly used in airplane design with many advantages, such as the high strength-to-weight and stiffness-to-weight ratios and the anisotropic nature in favor of aeroelastic tailoring. Aeroelastic tailoring usually involves the design optimization of a lifting surface to achieve desired aeroelastic responses, such as the maximizing of flutter and divergence speeds and the improvement of lift and control effectiveness. As one of the failure modes for the high-strength materials, crack initiation and propagation due to the manufacturing process or fatigue and impact loading during service has long been an important topic in composite and fracture mechanics communities [1]. It is also recognized that composite wing designers need to be aware of possible damage conditions at the beginning of a design involving the aeroelastic tailoring [2,3].

The current research was motivated by the fracture of composite wings in some unmanned aerial vehicles (UAVs) deployed in the last few years, such as the Predator [4]. The relative large wing span and high aspect ratio are the usual design for the low-speed UAVs. Surface cracks near the wing root are suspected as the main fracture failure for the aircraft under cyclic loading during normal flight or impact loading during maneuvering, taking off, and landing. It is of great value to investigate the influence of cracks on aeroelastic boundaries of a composite wing. Compared with vast research in aeroelastic tailoring and fracture mechanics of composite materials, the effects of damage on aeroelastic stabilities have been studied by only a few researchers. Chen and Lin [5] used finite element methods for the flutter characteristics of thin cracked panels. The existence of an edge crack decreases the flutter speed. Kapania and Castel [6] developed a one-dimensional finite element to study the aeroelastic behavior of unsymmetric composite wings with and without damage. The damage is modeled with a complete loss of stiffness for certain plies. The effect of transverse shear and bending–stretching coupling is considered. It is found that unsymmetry due to damage could decrease flutter and divergence speeds for certain fiber angles. Strganac and Kim [7] integrated a damage growth scheme to study the aeroelastic behavior of damaged composite plates. Damage is distributed in the form of matrix cracking in each ply, and a damage parameter is formulated to represent the crack density. The governing equations are solved in the time domain. With damage growth, the flutter boundary is first reduced and then leveled off at a certain damage level. The aeroelastic response depends also on the distribution of damage. Bauchau et al. [8] also studied the effect of matrix cracking on flutter characteristics of a composite wing. They concluded that matrix damage does not have significant influence on the flutter speed, but increases the amplitude of aeroelastic oscillations significantly. Realizing that matrix cracking is limited to cross-ply laminates in previous studies, Kim et al. [9] used finite difference and finite element methods to investigate bilinear flutter oscillations of damaged composite plates with angle-ply laminates. Aeroelastic stability is degraded due to the matrix cracking. The

Received 9 December 2005; revision received 29 November 2006; accepted for publication 16 December 2006.

*Postdoctoral Associate, Department of Mechanical Engineering, Center for Intelligent Material Systems and Structures. Member AIAA.

†Professor, Department of Mechanical Engineering, and Director, Center for Intelligent Material Systems and Structures. Fellow AIAA.

degradation is further enhanced by the decrease of the bending–torsion coupling level resulting from the matrix cracking. However, the effect of an edge crack on the aeroelastic behavior of composite wings has not been addressed to date.

In addition to a proper aerodynamic model, an accurate and computationally effective model of the composite wing is fundamental to secure reliable results in aeroelastic analysis. Although finite element methods are powerful in many aspects, they are most often too expensive to be coupled with other constrains to provide similar level of details for the preliminary design phase, and so a reduced analytical model is still desired to provide insights on aeroelastic phenomena with the total number of states kept as low as possible [10]. It is quite common that one-dimensional beam models with two independent variables (bending and torsion) are used as the analytical method to study the basic aeroelastic phenomena [11,12]. Similarly, it is the most popular approach in the literature to model a composite wing with a one-dimensional beam or box-beam model, for instance, Stein and Housner [13], Weisshaar [14,15], and Lottati [16]. Weisshaar and Foist [17] calculated the stiffness parameter of bending and torsion, as well as the coupling term for two different assumptions: zero chordwise moment and zero chordwise curvature (chordwise rigidity). It is shown that the beam model characterized by EI, GJ, and K is reasonably equivalent to the box-beam model that is usually believed more accurate in modeling composite wings. The beam model is widely used (e.g., Guo et al. [18]) in investigating the effect of laminate layup on the flutter speed of a composite wing. It should be noted, however, that two-dimensional thin-walled models (or even one-dimensional box-beam models developed in the last decades) can be very complicated, depending on whether one or more considerations are given on the coupling effects between the extension, in-plane and out-plane bending, twisting, warping of cross section, shear deformation, and rotary inertia. For instance, analytical thin-walled closed-section models of various complicities were investigated by Rehfield et al. [19], Chandra et al. [20], Smith and Chopra [21], and Dancila and Armanios [22]. On the other hand, in the context of aeroelasticity, the aerodynamic loading can also be modeled with increasingly more sophisticated effects based on assumptions that may vary between two-dimensional incompressible flow and three-dimensional unsteady flow. Therefore, combining the structural model with the aerodynamic model to solve the aeroelastic problem for an analytical solution could be very challenging (e.g., Librescu and Song [23] and Qin et al. [24]).

For the aforementioned reasons, simple structural and aerodynamic models are proposed in the present study to provide insight on the primary effect of cracks on a composite wing. The one-dimensional beam model presented by the authors earlier [25] in investigating vibration characteristics of cracked composite beams is selected as the basic elastic model of an aircraft composite wing. The wing is assumed to be unswept, with a large aspect ratio and uniform cross-section. The elastic coupling between bending and torsion modes is introduced by the unbalanced laminates. In addition, the offset of the center of gravity from the reference axis introduces an inertial coupling between the two modes, as recognized in most wing structures. The final equation of motion includes the coupling of both types. Other elastic interactions (such as extension-bending coupling, warping of cross section, rotary inertia, and shear deformation) are relatively less significant and are therefore neglected. The edge crack introduces additional boundary conditions at the crack location. The local flexibility matrix has the same components as determined in [25]. Steady and quasi-steady aerodynamic forces are assumed in calculating flutter and divergence speeds, considering the fact that many UAVs with slender composite wings fly at relatively low speed. Unidirectional fiber orientation is used to better understand the effect of material properties in conjunction with the edge crack. The fundamental mode shapes of both the intact and cracked beam are used in Galerkin's method to provide an approximate solution for flutter and divergence speeds. Free vibration of the cracked composite wing is analyzed. Finally, changes in the flutter/divergence speed (with respect to the crack ratio, its location, and the fiber orientation) are presented.

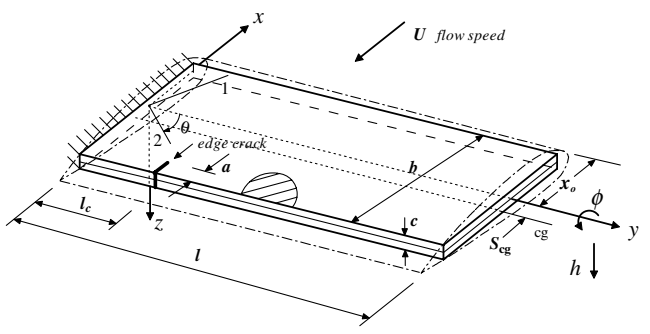

Fig. 1 A cantilever beam model for an unswept composite wing with an edge crack.

Modeling a Cracked, Unswept Composite Wing

The unswept composite wing modeled by a cantilever beam with uniform cross section is shown in Fig. 1, in which a transverse edge crack has a uniform depth and a crack plane parallel to the x–z plane. The 1–2 axes are the material's principal axes in each ply and at an angle of θ with respect to the x–y axes. The fiber angle in each ply, as well as the ply sequence, does not affect the formulation of the beam model. However, without losing generality, it is assumed that the fiber in each ply is orientated in the same direction, to investigate the effect of material properties on the flutter/divergence speed in the presence of the edge crack.

The bending stiffness parameter, the torsional stiffness parameter, and the bending–torsion coupling parameter are formulated the same way as in [25]. Once these parameters are obtained, free vibration of the composite wing model with damping neglected becomes

$$\begin{aligned} EI\frac{\partial^4 h}{\partial y^4} - K\frac{\partial^3 \phi}{\partial y^3} + m\frac{\partial^2 h}{\partial t^2} + S_y\frac{\partial^2 \phi}{\partial t^2} = 0 \\ GJ\frac{\partial^2 \phi}{\partial y^2} - K\frac{\partial^3 h}{\partial y^3} - I_y\frac{\partial^2 \phi}{\partial t^2} - S_y\frac{\partial^2 h}{\partial t^2} = 0 \end{aligned} \tag{1}$$

where $I_y = I_{cg} + mS_{cg}^2$ and $S_y = mS_{cg}$. Note that with the inertia axis parallel to the reference axis (the y axis) at a constant distance S_{cg}, Eq. (1) now includes the additional inertia coupling term containing S_y, compared with the composite beam Eq. 13 in [25].

Appendix A provides the analytical solution for the transverse displacement $H(y)$ and twisting angle $\Phi(y)$, along with the expression for cross-sectional rotation, bending moment, shear force, and torsional moment.

Let $\xi = y/l$ and the edge crack be located at $\xi_c = l_c/l$, as shown in Fig. 1. The beam can be replaced with two intact beams connected at the crack location. Let $\Gamma = [\cosh\alpha\xi \quad \sinh\alpha\xi \quad \cos\beta\xi \quad \sin\beta\xi \quad \cos\gamma\xi \sin\gamma\xi]^T$; the transverse displacement $H(\xi)$ can then be expressed as

$$H(\xi) = \begin{cases} H_1(\xi) = [A_1 \quad A_2 \quad A_3 \quad A_4 \quad A_5 \quad A_6]\Gamma & 0 \le \xi \le \xi_c \\ H_2(\xi) = [A_7 \quad A_8 \quad A_9 \quad A_{10} \quad A_{11} \quad A_{12}]\Gamma & \xi_c < \xi \le 1 \end{cases} \tag{2a}$$

and, accordingly, the twisting angle is

$$\Phi(\xi) = \begin{cases} \Phi_1(\xi) = [B_1 \quad B_2 \quad B_3 \quad B_4 \quad B_5 \quad B_6]\Gamma & 0 \le \xi \le \xi_c \\ \Phi_2(\xi) = [B_7 \quad B_8 \quad B_9 \quad B_{10} \quad B_{11} \quad B_{12}]\Gamma & \xi_c < \xi \le 1 \end{cases} \tag{2b}$$

There are 12 unknowns in Eq. (2), because $B_{1–12}$ are related to $A_{1–12}$ by the relationship in Eq. (A4). At the crack location $\xi = \xi_c$, the local flexibility concept demands

$$M_1(\xi_c) = M_2(\xi_c) \tag{3a}$$

$$S_1(\xi_c) = S_2(\xi_c) \tag{3b}$$

$$T_1(\xi_c) = T_2(\xi_c) \tag{3c}$$

$$H_2(\xi_c) = H_1(\xi_c) + c_{22}S_1(\xi_c) + c_{26}T_1(\xi_c) \tag{3d}$$

$$\Theta_2(\xi_c) = \Theta_1(\xi_c) + c_{44}M_1(\xi_c) \tag{3e}$$

$$\Phi_2(\xi_c) = \Phi_1(\xi_c) + c_{62}S_1(\xi_c) + c_{66}T_1(\xi_c) \tag{3f}$$

$$\text{with} \quad [C] = \begin{bmatrix} c_{22} & 0 & c_{26} \\ 0 & c_{44} & 0 \\ c_{62} & 0 & c_{66} \end{bmatrix}, \quad \text{where } c_{26} = c_{62}$$

The local flexibility matrix $[C]$ is the same as expressed in Eq. 9 in [25], with components given in Eq. 8 of the same reference. For a cantilever wing, the fixed-free boundary conditions require that at the fixed end, $\xi = 0$,

$$H_1(0) = 0 \tag{4a}$$

$$\Theta_1(0) = 0 \tag{4b}$$

$$\Phi_1(0) = 0 \tag{4c}$$

and at the free end, $\xi = 1$

$$M_2(1) = 0 \tag{4d}$$

$$S_2(1) = 0 \tag{4e}$$

$$T_2(1) = 0 \tag{4f}$$

Substitution of Eq. (2) into Eqs. (3) and (4) yields the characteristic equation:

$$[\Lambda]A = 0 \tag{5}$$

where
$A =$
$[A_1 \quad A_2 \quad A_3 \quad A_4 \quad A_5 \quad A_6 \quad A_7 \quad A_8 \quad A_9 \quad A_{10} \quad A_{11} \quad A_{12}]^T$
and $[\Lambda]$, the 12×12 characteristic matrix being a function of frequency. Natural frequencies can be obtained by solving equations $\det[\Lambda] = 0$. Substituting each natural frequency back into Eq. (5) yields the corresponding mode shape. Here, the bending-torsion coupling is permanently present due to the inertial coupling, even though the elastic coupling vanishes when fiber angle $\theta = 0$ or 90 deg, as shown in [25].

Aeroelastic Stability of the Cracked Composite Wing

Because the flight speed is presumed to be low enough and little vortex could be produced due to the low angle of attack and small displacements, only incompressible flow is considered in this study to formulate an aerodynamic model. It should be noted that a subsonic or supersonic aerodynamic model shall be applied if the composite wing is in high-speed airflow. Furthermore, the large aspect ratio also justifies the use of two-dimensional strip theory. Under these circumstances, the lifting force and pitching moment per unit span by a quasi-steady aerodynamic model may be expressed as [12]

$$\begin{aligned} L &= \frac{\rho U^2}{2}\frac{\partial C_L}{\partial \phi} b\left[\phi + \frac{1}{U}\frac{\partial h}{\partial t} + \frac{b}{U}\left(\frac{3}{4} - \frac{x_o}{b}\right)\frac{\partial \phi}{\partial t}\right] \\ M &= \frac{\rho U^2}{2}\frac{\partial C_L}{\partial \phi} b^2\left(\frac{x_o}{b} - \frac{1}{4}\right)\left[\phi + \frac{1}{U}\frac{\partial h}{\partial t} + \frac{b}{U}\left(\frac{3}{4} - \frac{x_o}{b}\right)\frac{\partial \phi}{\partial t}\right] \\ &\quad - \frac{\rho U b^3 \pi}{16}\frac{\partial \phi}{\partial t} \end{aligned} \tag{6}$$

where C_L has the theoretical value $\partial C_L/\partial\phi = 2\pi$. If the effective angle of attack contribution is neglected, the slightly less complex counterparts by a steady aerodynamic model can be expressed as [26]

$$L = \frac{\rho U^2}{2}\frac{\partial C_L}{\partial \phi} b\phi, \qquad M = Lb\left(\frac{x_o}{b} - \frac{1}{4}\right) \tag{7}$$

The equation of motion of the composite wing with aerodynamic forces applied becomes

$$\begin{aligned} EI\frac{\partial^4 h}{\partial y^4} - K\frac{\partial^3 \phi}{\partial y^3} + m\frac{\partial^2 h}{\partial t^2} + S_y\frac{\partial^2 \phi}{\partial t^2} + L = 0 \\ GJ\frac{\partial^2 \alpha}{\partial y^2} - K\frac{\partial^3 h}{\partial y^3} - I_y\frac{\partial^2 \phi}{\partial t^2} - S_y\frac{\partial^2 h}{\partial t^2} + M = 0 \end{aligned} \tag{8}$$

Substituting Eq. (6) into Eq. (8) yields the governing equation with quasi-steady aerodynamic forces as

$$\begin{aligned} &EI\frac{\partial^4 h}{\partial y^4} - K\frac{\partial^3 \phi}{\partial y^3} + m\frac{\partial^2 h}{\partial t^2} + S_y\frac{\partial^2 \phi}{\partial t^2} + L_1 U\left(\frac{\partial h}{\partial t} + U\phi\right) + L_2 U\frac{\partial \phi}{\partial t} \\ &\quad = 0 \\ &GJ\frac{\partial^2 \alpha}{\partial y^2} - K\frac{\partial^3 h}{\partial y^3} - I_y\frac{\partial^2 \phi}{\partial t^2} - S_y\frac{\partial^2 h}{\partial t^2} + M_1 U\left(\frac{\partial h}{\partial t} + U\phi\right) + M_2 U\frac{\partial \phi}{\partial t} \\ &\quad = 0 \end{aligned} \tag{9}$$

where

$$\begin{aligned} L_1 &= \frac{\rho b}{2}\frac{\partial C_L}{\partial \phi}, \qquad M_1 = \frac{\rho b^2}{2}\frac{\partial C_L}{\partial \phi}\left(\frac{x_o}{b} - \frac{1}{4}\right) \\ L_2 &= L_1 b\left(\frac{3}{4} - \frac{x_o}{b}\right), \qquad M_2 = M_1 b\left(\frac{3}{4} - \frac{x_o}{b}\right) - \frac{\rho b^3 \pi}{16} \end{aligned}$$

Substituting Eq. (7) into Eq. (8) reduces the governing equation for steady aerodynamic forces to

$$\begin{aligned} EI\frac{\partial^4 h}{\partial y^4} - K\frac{\partial^3 \phi}{\partial y^3} + m\frac{\partial^2 h}{\partial t^2} + S_y\frac{\partial^2 \phi}{\partial t^2} + L_1 U^2\phi = 0 \\ GJ\frac{\partial^2 \alpha}{\partial y^2} - K\frac{\partial^3 h}{\partial y^3} - I_y\frac{\partial^2 \phi}{\partial t^2} - S_y\frac{\partial^2 h}{\partial t^2} + M_1 U^2\phi = 0 \end{aligned} \tag{10}$$

The linear homogeneous Eqs. (9) and (10) may have a solution in the following form:

$$h(y,t) = Af(y)e^{\lambda t}, \qquad \phi(y,t) = Bg(y)e^{\lambda t} \tag{11}$$

where A, B, and l are complex constants, in general.

Because the flutter modes are not known at the beginning, an approximate solution by Galerkin's method is usually obtained by assuming that the functions $f(y)$ and $g(y)$ are real and satisfy the boundary conditions so that they can be taken as the fundamental mode shapes of free vibration. Similarly, it is natural for the cracked beam model to assume that $f(y)$ and $g(y)$ are the fundamental mode shapes satisfying boundary conditions, not only at the ends, but also at the crack location. The real functions $f(y)$ and $g(y)$ are now piecewise continuous with a discontinuity at the crack location. Because both $f(y)$ and $g(y)$ satisfy the boundary condition at the

crack location, they carry most of the information related directly to the presence of the crack. Meanwhile, because the aerodynamic forces are derived from two-dimensional strip theory, they are determined by the airfoil and angle of attack at each cross section; the aerodynamic forces at one cross section do not affect the forces at other cross sections. In other words, the discontinuity of $f(y)$ and $g(y)$ does not affect the validation of the aerodynamic forces as given in Eqs. (6) or (7). In the following analysis, functions $f(y)$ and $g(y)$ are taken as the fundamental bending and torsional mode shapes, respectively. They are obtained during the free vibration analysis presented in the last section. Note that $f(y)$ and $g(y)$ are not decoupled bending and torsional mode shapes (as widely used in the preliminary aeroelastic analysis of a wing structure), but coupled mode shapes at the first natural frequency. Using coupled modes as trial functions certainly provides more accurate solutions than the decoupled modes in aeroelastic analysis [12].

Substituting Eq. (11) into Eq. (9) for the quasi-steady aerodynamic model and eliminating $e^{\lambda t}$ yields

$$A[EIf^{iv} + f(m\lambda^2 + L_1\lambda U)] + B[-Kg''' + g(L_1U^2 + S_y\lambda^2 + L_2\lambda U)] = 0 \tag{12a}$$

$$A[Kf''' + f(S_y\lambda^2 - M_1\lambda U)] + B[-GJg'' - g(M_1U^2 - I_y\lambda^2 + M_2\lambda U)] = 0 \tag{12b}$$

Similarly, substituting Eq. (11) into Eq. (10) reduces Eq. (12) for the steady aerodynamic model, as

$$A[EIf^{iv} + \lambda^2 mf] + B[-Kg''' + \lambda^2 S_y g + L_1U^2 g] = 0 \tag{13a}$$

$$A[-Kf''' - \lambda^2 S_y f] + B[GJg'' - \lambda^2 I_y g + M_1U^2 g] = 0 \tag{13b}$$

The coupled bending and torsional mode shapes for the cracked wing model can be expressed, respectively, as

$$f(y) = \begin{cases} f_1(y) & 0 \le y \le l_c \\ f_2(y) & l_c < y \le l \end{cases}, \qquad g(y) = \begin{cases} g_1(y) & 0 \le y \le l_c \\ g_2(y) & l_c < y \le l \end{cases} \tag{14}$$

where $f_1(y)$, $f_2(y)$, $g_1(y)$, and $g_2(y)$ are all continuous within the individual domain. Multiplying Eq. (12a) by $f(y)$ and Eq. (12b) by $g(y)$ and integrating over $[0, l]$ yields

$$\begin{aligned} A[a_{11} + c_{11}\lambda^2 + d_{11}\lambda U] + B[a_{12} + b_{12}U^2 + c_{12}\lambda^2 + d_{12}\lambda U] = 0 \\ A[a_{21} + c_{21}\lambda^2 + d_{21}\lambda U] + B[a_{22} + b_{22}U^2 + c_{22}\lambda^2 + d_{22}\lambda U] = 0 \end{aligned} \tag{15}$$

where coefficients a_{11} to d_{22} are given in Appendix B. A nontrivial solution of Eq. (15) requires that

$$\det\begin{bmatrix} a_{11} + c_{11}\lambda^2 + d_{11}\lambda U & a_{12} + b_{12}U^2 + c_{12}\lambda^2 + d_{12}\lambda U \\ a_{21} + c_{21}\lambda^2 + d_{21}\lambda U & a_{22} + b_{22}U^2 + c_{22}\lambda^2 + d_{22}\lambda U \end{bmatrix} = 0$$

or

$$A_1\lambda^4 + B_2U\lambda^3 + (B_1 + C_1U^2)\lambda^2 + (D_2U + F_2U^3)\lambda + D_1 + F_1U^2 = 0 \tag{16}$$

Equation (16) can be further rewritten as

$$A_0\lambda^4 + B_0\lambda^3 + C_0\lambda^2 + D_0\lambda + E_0 = 0 \tag{17}$$

Coefficients A_1 to F_1 in Eq. (16) and A_0 to E_0 in Eq. (17) are given in Appendix B. For the steady aerodynamic model, Eq. (15) reduces to

$$\begin{aligned} A[a_{11} + c_{11}\lambda^2] + B[a_{12} + b_{12}U^2 + c_{12}\lambda^2] = 0 \\ A[a_{21} + c_{21}\lambda^2] + B[a_{22} + b_{22}U^2 + c_{22}\lambda^2] = 0 \end{aligned} \tag{18}$$

such that the characteristic equation becomes

$$A_1\lambda^4 + (B_1 + C_1U^2)\lambda^2 + D_1 + F_1U^2 = 0 \tag{19}$$

that can be further rewritten as

$$A_0\lambda^4 + C_0\lambda^2 + E_0 = 0 \tag{20}$$

Flutter/Divergence Speed by Quasi-Steady Aerodynamic Forces

The stability condition requires that all roots of Eq. (17) have negative real parts. The necessary and sufficient condition is that the coefficients A_0, B_0, C_0, D_0, and E_0 and the Routh discriminant

$$R = B_0C_0D_0 - B_0^2E_0 - D_0^2A_0$$

have the same sign [12]. Because $A_0 = A_1$ is always positive, the stability condition becomes

$$B_0 > 0, \qquad C_0 > 0, \qquad D_0 > 0, \qquad E_0 > 0 \quad \text{and} \quad R > 0 \tag{21}$$

Because E_0 and R become zero before either B_0, C_0, or D_0 does with increasing air speed, the stability condition can be further simplified to evaluate the signs of E_0 and R. At the critical condition, $E_0 = 0$ and/or $R = 0$.

1) If $E_0 = 0$, Eq. (17) has a root $\lambda = 0$, which results in the divergence speed, as

$$U_{\text{div}}^2 = -\frac{D_1}{F_1} = \frac{a_{12}a_{21} - a_{11}a_{22}}{a_{11}b_{22} - a_{21}b_{12}} \tag{22}$$

2) If $R = 0$, substitution of B_0, C_0, D_0, and E_0 for R yields

$$U^2(JU^4 + MU^2 + N) = 0 \tag{23}$$

where $J = B_2C_1F_2 - A_1F_2^2$, $M = B_2C_1D_2 - B_2^2F_1 + B_1B_2F_2 - 2A_1D_2F_2$, and $N = B_1B_2D_2 - B_2^2D_1 - A_1D_2^2$.

The solution $U = 0$ in Eq. (23) is trivial, because it only indicates that the beam has a harmonic response in still air. The actual flutter speed can be determined from Eq. (23) to be

$$U_{\text{flutt}}^2 = -\frac{M}{2J} \pm \frac{1}{2J}\sqrt{M^2 - 4JN} \tag{24}$$

where the smaller positive value corresponds to the critical flutter speed.

In the cases that $F_1 = 0$ or $D_1/F_1 > 0$ in Eq. (22), or $J = 0$ or M^2–$4JN < 0$ in Eq. (24), the stability condition can be determined from the criterion (21) by calculating all coefficients in Eq. (17) with a slightly increased air speed above zero. This may result in infinite (or zero) divergence/flutter speed, indicating aerodynamically stable (or unstable) motion in each situation. The flutter instability is usually reached first in the design of an aircraft wing. However, in some cases (such as when the fibers are orientated at a certain angle), divergence can occur first; thus, divergence needs to be considered as well.

Flutter/Divergence Speed by Steady Aerodynamic Forces

For nonzero A_0, Eq. (20) has a solution in the following form:

$$\lambda^2 = \frac{-C_0 \pm \sqrt{C_0^2 - 4A_0E_0}}{2A_0} \tag{25}$$

Solving Eq. (20) for λ^2 yields a pair of real or complex values, depending on the sign of $C_0^2 - 4A_0E_0$. Because the system has no damping, as shown in the governing Eq. (10), a solution of $h(y, t)$ and $\phi(y, t)$ is stable only in the case that all values of λ^2 are purely real and negative. A positive real value of λ^2 yields a positive real root of

λ in Eq. (20), whereas a complex value of λ^2 yields that at least one root of λ has a positive real part; both indicate an unstable motion. Meanwhile, it can be shown easily that $A_0 = A_1$ is a positive constant, not depending on air speed. Therefore, a stable solution requires that the following coefficients must be all positive simultaneously:

$$C_0 > 0, \qquad E_0 > 0, \qquad C_0^2 - 4A_0E_0 > 0 \tag{26}$$

When the air speed U increases from zero, C_0, E_0, and $C_0^2 - 4A_0E_0$ must be all greater than zero for a stable motion. With the increasing of U, it is obvious that either E_0 or $C_0^2 - 4A_0E_0$ will become zero before C_0 does, if the system becomes unstable. Hence, it is only required to check the signs of E_0 and $C_0^2 - 4A_0E_0$. At the critical speed, $E_0 = 0$ or $C_0^2 - 4A_0E_0 = 0$.

1) If $E_0 = 0$, Eq. (20) has a root $\lambda = 0$, which results in the same divergence speed as in Eq. (22).

2) If $C_0^2 - 4A_0E_0 = 0$, substitution of C_0, A_0 and E_0 in Eq. (20) yields

$$RU^4 + SU^2 + T = 0 \tag{27}$$

where $R = C_1^2$, $S = 2(B_1C_1 - 2A_1F_2)$, and $T = B_1^2 - 4A_1D_1$. The flutter speed can then be determined from Eq. (27) to be

$$U_{\text{flutt}}^2 = -\frac{S}{2R} \pm \frac{1}{2R}\sqrt{S^2 - 4RT} \tag{28}$$

where the smaller positive value corresponds to the critical flutter speed. Following the same procedure aforementioned to calculate coefficients in Eq. (20) from the criterion (26) for cases that $R = 0$ or S^2–$4RT < 0$ in Eq. (28), the stability condition can be finally determined.

Results

The composite beam consists of several plies aligned in the same direction. In each ply, the material is assumed orthotropic with respect to its axes of symmetry. Material properties of each ply are taken to be the same as in [25]. Although the three elastic parameters EI, GJ, and K are calculated directly form the beam model, they are equivalent to those obtained by a box-beam model and can be further determined numerically or experimentally by a real composite wing structure. Values from a real composite wing certainly benefit the analysis, affecting the actual flutter/divergence speed. However, the present research does not aim at an accurate calculation of either flutter or divergence speed; instead, the focus is on the variation or rate of variation in the presence of a surface crack and to establish trends that could be useful in design. Therefore, the variation of flutter and divergence speeds predicted by Galerkin's method here for an intact wing with respect to different fiber angles should be treated as an estimate, rather than an accurate mapping. The model geometry of the cantilever wing is taken to be length $l = 1.0$ m, width $b = 0.25$ m, thickness $c = 0.02$ m, and offset of the center of gravity $S_{\text{cg}} = 0.05$ m.

Some Plots for the Wing Without Cracks

It may be of interest to first explore the variation of the three elastic parameters, natural frequencies, and flutter/divergence speed with respect to fiber angles for the beam without any cracks. Figure 2 illustrates the variation of EI, GJ, K, and $\Psi(=K/\sqrt{EI \cdot GJ})$ for fiber angles between 0 and 180 deg. Figure 3 shows the variation of the first four natural frequencies for the same range of fiber angles. Figure 4 is the plot of normalized flutter and divergence speeds for steady aerodynamic forces; the same plot for quasi-steady aerodynamic forces is shown in Fig. 5.

Figure 2 indicates the symmetry of EI and GJ and antisymmetry of K and Ψ with respect to the fiber angle at 90 deg (or 0 deg), which is expected as the same characteristics presented in [25]. The symmetry of natural frequencies with respect to the fiber angle at 90 deg was first presented in [26] with a box-beam composite wing and later indicated in [27]. However, the symmetric nature of natural

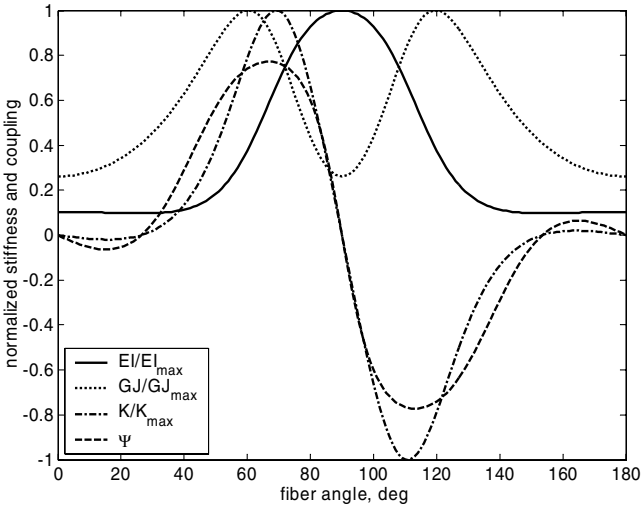

Fig. 2 Variation of the elastic parameters EI, GJ, K, and Ψ with respect to fiber angles.

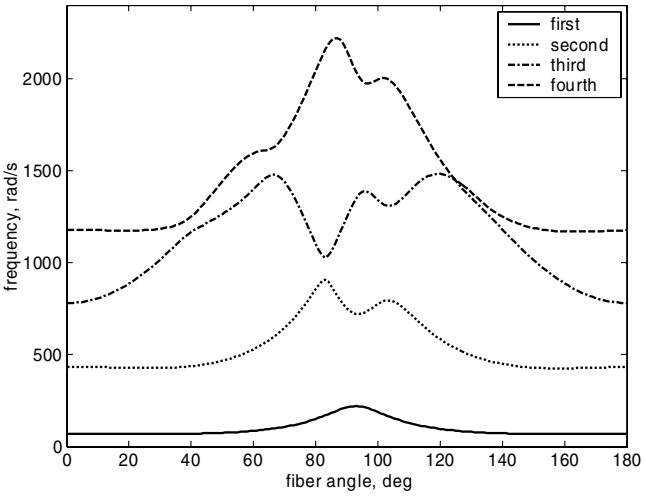

Fig. 3 Variation of the first four natural frequencies with respect to fiber angles.

frequencies for beams without the inertia coupling no longer exists for the wing model including the inertia coupling, except for the very first natural frequency, as shown in Fig. 3. The lowest mode is predominantly controlled by the bending mode during the variation

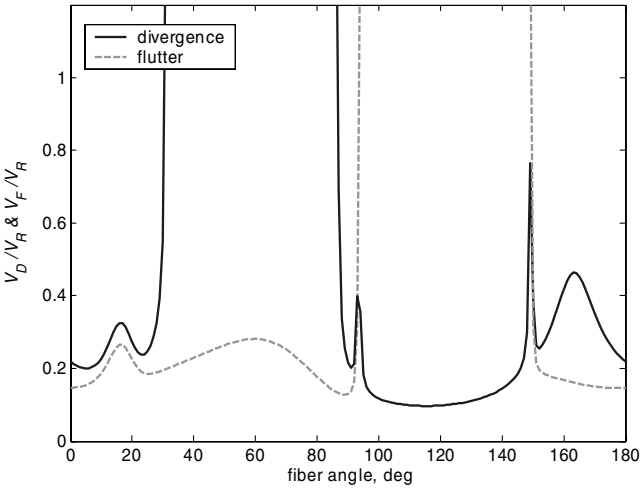

Fig. 4 Variation of flutter and divergence speeds with respect to fiber angles (steady aeroforces).

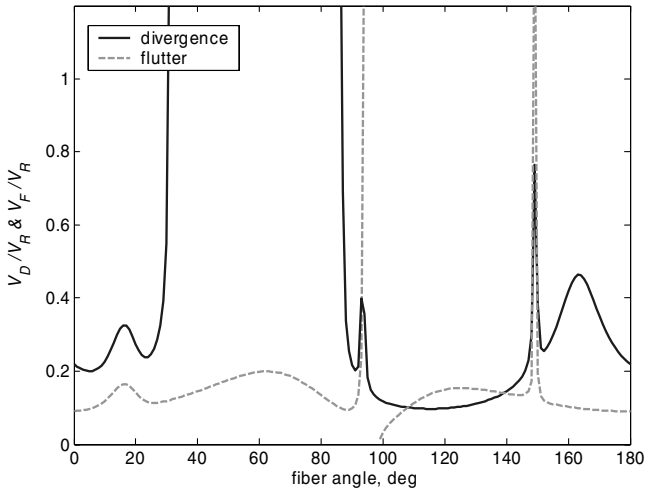

Fig. 5 Variation of flutter and divergence speeds with respect to fiber angles (quasi-steady aeroforces).

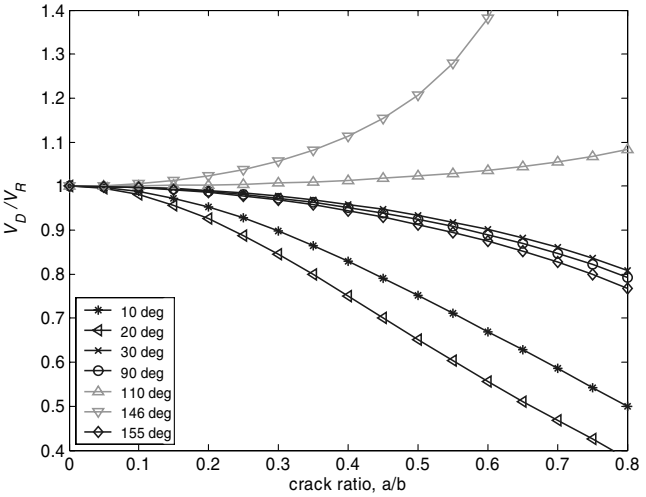

Fig. 6 Variation of divergence speed with respect to the crack ratio.

of fiber angles. Plots of higher modes show the effect that either the bending or torsional mode is no longer in the shape of a certain mode but "distorted" to some extent, especially in the range that two consecutive frequencies are close to each other. However, for the variation of the lowest frequency, both the bending and torsional modes bear the shape of its first mode. The lowest coupled bending and torsional modes will be selected in the following analysis, for both the intact and cracked beams.

In Figs. 4 and 5, V_D and V_F represent the divergence speed and flutter speed, respectively, and V_R is a reference speed selected to normalized V_D and V_F. Although the divergence speed is the same for either steady or quasi-steady aerodynamic models, flutter speeds predicted by the steady aerodynamics model are about 60% higher than those by the quasi-steady aerodynamic model for fiber angles less than 50 deg or greater than 149 deg and about 35% higher for fiber angles between 50 and 94 deg. Flutter speeds predicted by the steady aerodynamic model are much less conservative. Another significant difference is that the quasi-steady aerodynamic model predicts flutter instabilities for fiber angles between 94 and 149 deg, with a severe instability around 97 deg, whereas the steady aerodynamic model indicates no flutter for the same range of fiber angles. Flutter speeds can be higher or lower than divergence speeds, depending on the range of fiber angles; either speed can go to infinity at a certain range of fiber angles. The same phenomena were also observed by Cesnik et al. [10], who investigated variation of flutter and divergence speeds of composite wing with box-beam models. Moreover, changing the reference axis location or inertia axis location significantly affects both divergence and flutter curves in the way that the curves are not only shifted, but also "reshaped." The inertia axis ahead of the reference axis (with a negative S_{cg} value) tends to improve aerodynamic stabilities by increasing both flutter and divergence speeds for the same range of fiber angles, which is the same phenomenon for conventional wing structures [28]. The current research assumes that the reference axis is located in the leading half-chord, with the distance to the leading edge as $x_o = 0.45b$, close to the centerline, and the inertia axis is $0.2b$ aft. This is a reasonable assumption for a cantilever composite wing with a large aspect ratio.

Effects of Crack Ratios and Fiber Angles

The edge crack reduces the stiffness of the composite wing such that the global vibration modes are disturbed. The disturbance is not equally exerted on the coupled bending mode or torsional mode, as indicated in the case of no inertia coupling in [25]. A plot of the first coupled bending and torsional modes (in terms of the crack ratio) indicates that the bending mode is always disturbed more than the torsional mode, due to the crack.

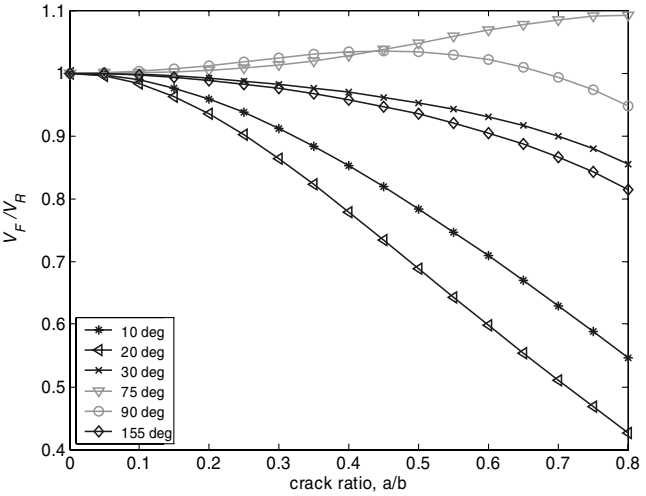

Fig. 7 Variation of flutter speed with respect to the crack ratio (steady aeroforces).

To investigate the effects of cracks on the flutter/divergence speed at different fiber angles, the following 9 fiber angles are selected: 10, 20, 30, 75, 90, 110, 130, 146, and 155 deg. The selection is based on the variation of flutter speed shown in Figs. 4 and 5. A fiber angle is chosen for the range in which the flutter speed increases or decreases.

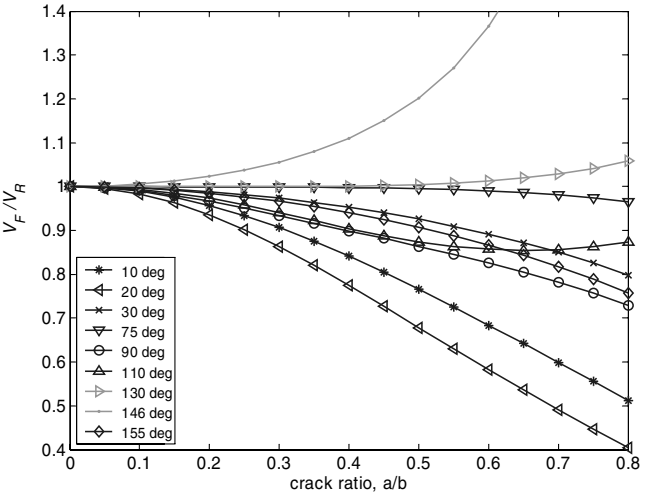

Fig. 8 Variation of flutter speed with respect to the crack ratio (quasi-steady aeroforces).

Table 1 Elastic parameters and the first two natural frequencies of the intact wing

Fiber angle	EI, N · m^2	GJ, N · m^2	Ψ, N · m^2	First natural frequency, rad/s	Second natural frequency, rad/s
$\theta = 20$ deg	3635.2	7537.1	−0.054	69.8	429.1
$\theta = 146$ deg	3722.3	11391.3	−0.132	70.5	435.9

For the crack located at $\xi_c = 0.2$, the normalized divergence speed with respect to the crack ratio is plotted in Fig. 6. Figures 7 and 8 illustrate the variation of flutter speeds. The corresponding speed in the absence of the crack is selected as the reference speed V_R.

The divergence speed shown in Fig. 6 tends to increase with the crack ratio increased for the fiber angles at 110 or 146 deg, whereas in any other situations, the divergence speed decreases with the increasing crack ratio. On the other hand, the flutter speed predicted by the steady aerodynamic model tends to increase slightly for fiber angles at 75 deg, with an increase–decrease variation for fiber angles at 90 deg. At any other fiber angles, the speed decreases with the increasing crack ratio. The flutter speed predicted by the quasi-steady aerodynamic model, however, decreases with the increasing crack ratio for most fiber angles. The rate of decrease is much higher for smaller fiber angles. An increase is only observed for the fiber angles at 130 and 146 deg, for which the steady aerodynamic model predicts no flutter instability. Recall that due to the existence of inertia coupling, mode shapes of the cracked beam are no longer symmetric when the fiber angle is symmetric by the reference axis. The change in divergence/flutter speed of the composite wing is now affected by the interaction of the crack ratio, the elastic bending-torsion coupling of the material, and the inertia bending-torsion coupling of the wing structure.

The phenomenon that a crack tends to increase divergence/flutter speeds at a certain range of fiber angles was also observed by Lin et al. [29] who investigated the aeroelastic stabilities of a cracked anisotropic panel. For a wing structure, the flutter instability usually occurs when two consecutive frequencies coalesce or tend to "merge" [11]. It is true that at any fiber angles and for a fixed crack (both magnitude and location), solving Eq. (17) for the quasi-steady aerodynamic model indicates that the first two critical frequencies tend to merge with increasing airspeed. However, with the directional stiffness changing with fiber angles, the presence of a crack may cause changes in mode shapes such that certain critical frequencies may be increased or remain unchanged, whereas other critical frequencies may be decreased. In other words, there exists the chance that a crack may result in two consecutive frequencies separating from, rather than merging with, each other.

To illustrate the crack effects further, two fiber angles (20 and 146 deg) are selected in solving Eq. (17) for critical frequencies with the quasi-steady aerodynamic model. When the wing has no cracks, there is no significant difference between elastic parameters and the first two natural frequencies for the two fiber angles, as shown in Table 1. For the airspeed that is fixed at 100 m/s (below the divergence and flutter speeds), Fig. 9 clearly indicates that with increasing crack ratio, the two critical frequencies [obtained by Eq. (17)] tend to coalesce for fiber angles at 20 deg and separate for fiber angles at 146 deg.

It should be noted that more rigorous modeling or experimental verification may be needed to justify that divergence/flutter speeds of a cracked composite wing at certain fiber angles tend to increase with an increasing crack ratio. Moreover, the cracked composite beam model, as well as the cracked composite wing model herein, is valid only for small cracks, because a larger crack may violate the assumption that the system is linear and involves only small displacements. Therefore, it is suggested that for a crack ratio larger than 0.5, predictions shown in all related plots should not be relied on for an accurate result.

Effects of Crack Locations and Fiber Angles

For the case in which the crack ratio is constant at $a/b = 0.3$, effects of the dimensionless crack location are shown in Fig. 10 for divergence speeds and Figs. 11 and 12 for flutter speeds.

For smaller fiber angles ($\theta = 10$ or 20 deg) in which the bending stiffness is low and the elastic coupling is weak, the lowest flutter and divergence speeds are found near the root of the wing. For the fiber angle larger than 30 deg, the overall variation in divergence speeds is within the 5% range. When the crack location moves along the wing span, the flutter speed predicted by the quasi-steady aerodynamic model usually does not change monotonically with the crack location. Whether a crack near the wing root reduces the flutter speed more than the crack at other locations is certainly affected by the elastic and inertia properties of the wing, and the question may not be answered simply by "yes" or "no." For a fixed crack ratio, the decrease of divergence/flutter speed might be precluded by implementing tailoring techniques. On the other hand, for certain fiber angles, further research is needed to justify the possibility that the shift of the crack location toward the composite wingtip can actually be accompanied by a decay of divergence/flutter speeds.

Conclusions

The aeroelastic characteristics of an unswept composite wing with an edge crack are investigated. The cracked wing is modeled by a cracked composite cantilever developed in [25], with inertia coupling terms included in the governing equations. The critical flutter and divergence speeds are obtained by Galerkin's method in which the fundamental mode shapes of the cracked beam in free vibration are used. The mode shapes satisfy all boundary conditions, including those at the crack location, and thus carry most of the information of the cracked beam for the final approximate solution.

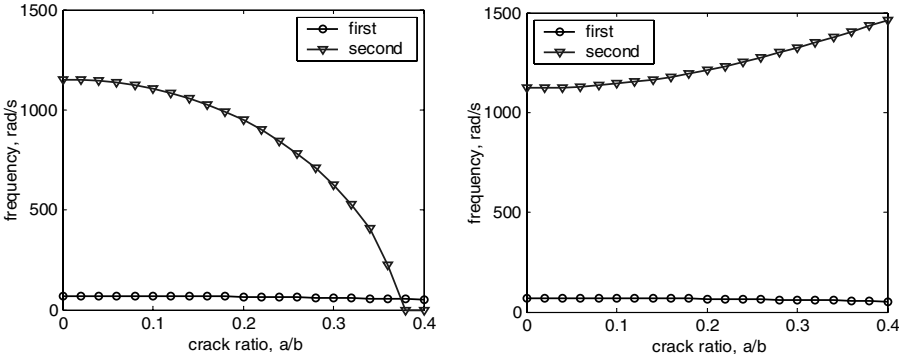

a) Fiber angle $\theta = 20$ deg **b) Fiber angle $\theta = 146$ deg**

Fig. 9 Variation of the two critical frequencies with respect to the crack ratio at a constant airspeed.

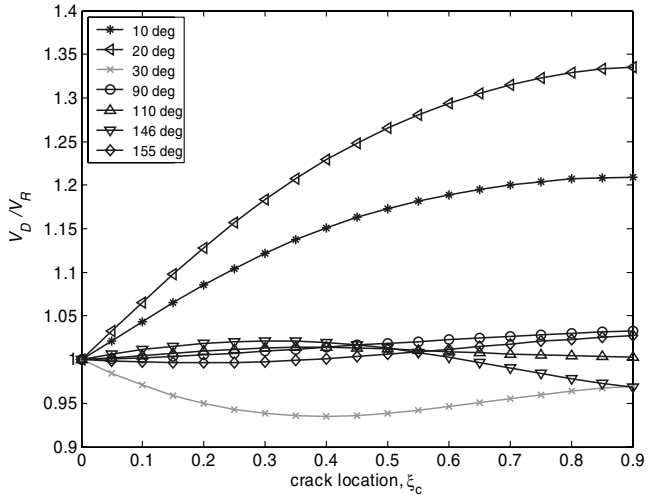

Fig. 10 Variation of divergence speed with respect to the crack location.

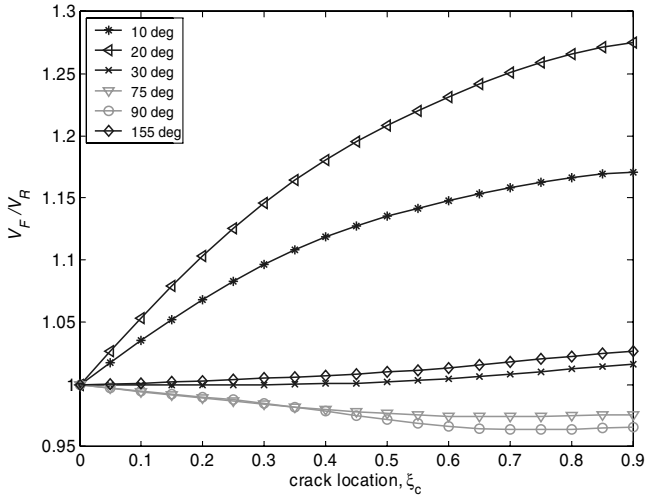

Fig. 11 Variation of flutter speed with respect to the crack location (steady aeroforces).

Both steady and quasi-steady aerodynamic forces are considered in the analysis.

The divergence/flutter speed varies with the reference axis location, the inertia axis location, fiber angles, and the crack ratio and location. For the reference axis fixed in the leading half-chord with the inertia axis aft, the divergence/flutter speed is more sensitive to the stiffness orientation than to the crack itself. At certain fiber angles, the presence of a crack tends to increase the flutter or divergence speed, a similar phenomenon as observed by Lin et al. [29]. The instability boundaries that are constant for an isotropic wing become alternating with the varying fiber angles of a composite wing, which is also observed by Lin et al. [30] for a composite plate in subsonic flow. The anisotropy of the composite wing introduces many completely different phenomena in the aeroelastic instability.

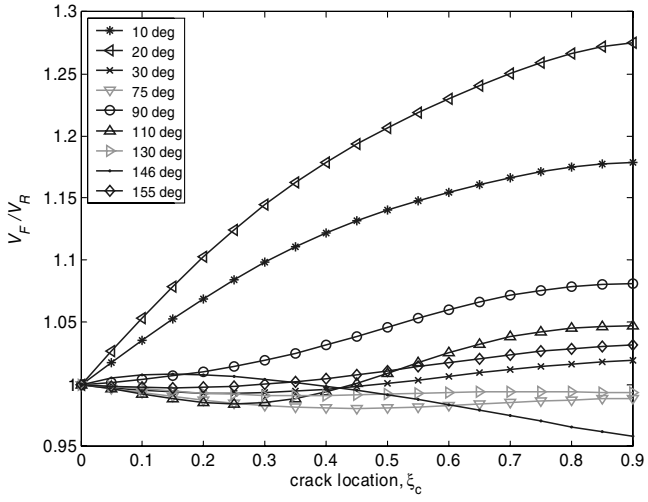

Fig. 12 Variation of flutter speed with respect to the crack location (quasi-steady aeroforces).

The flutter speed tends to increase as the crack ratio increases at certain fiber angles, which may need further investigation. However, in most situations, the flutter speed decreases with the increasing crack ratio, especially for that predicted by the quasi-steady aerodynamic model. The rate of change is higher with smaller fiber angles. Although an edge crack does not always reduce either flutter or divergence speed, it does reduce the stability boundaries in most cases, in terms of the stiffness orientation considered in the present research. As to a crack of fixed magnitude, the lowest flutter speed is observed when the crack approaches the root of the composite wing with smaller fiber angles. However, both flutter and divergence speeds experience variation with different crack locations, and the magnitude of variation with respect to the crack location is relatively small.

Once a crack is found on a composite wing, monitoring of the crack growth could be more critical to determining the aeroelastic stability of the wing, especially in the case for which the crack does not result in a flutter speed drop, due to certain fiber orientation. But in the case for which a crack does reduce the flutter speed, a fast drop in flutter speed might result in a catastrophic failure by a small crack that has not grown. When coupled with a crack-detection algorithm, the connection presented here between crack properties and flutter speed may be used as a damage prognosis tool to predict how the system will behave under future loading.

Appendix A: Analytical Solution of Eq. (1)

Based on separation of variables $h(y,t) = H(y)e^{i\omega t}$, $\phi(y,t) = \Phi(y)e^{i\omega t}$, Eq. (1) can be transferred to the eigenproblem

$$\begin{aligned} EI \cdot H^{iv} - K\Phi''' - \omega^2(mH + S_y\Phi) = 0 \\ GJ \cdot \Phi'' - KH''' + \omega^2(I_y\Phi + S_yH) = 0 \end{aligned} \tag{A1}$$

where the primes or superscript numerals indicate differentiation with respect to y. With $\xi = y/l$ and $D = \mathrm{d}(\cdot)/\mathrm{d}\xi$, eliminating either H or Φ in Eq. (A1) yields the auxiliary equation

$$(D^6 + uD^4 - vD^2 - uvw)W = 0 \tag{A2}$$

where $W = \Phi$ or H and

$$u = \frac{I_y EI \cdot l^2\omega^2}{EI \cdot GJ - K^2}, \qquad v = \frac{mGJ \cdot l^4\omega^2}{EI \cdot GJ - K^2}$$
$$w = \left(1 - \frac{S_y^2}{I_y m}\right)\left(1 - \frac{K^2}{EI \cdot GJ}\right)$$

Because $I_y = I_{cg} + mS_{cg}^2 > 0$ and $0 < K^2/(EI \cdot GJ) < 1$, it is obvious that $0 < w < 1$. Following the same procedure in [25], Eq. (A1) can be solved with a general solution as

$$\begin{aligned} H(\xi) &= A_1\cosh\alpha\xi + A_2\sinh\alpha\xi + A_3\cos\beta\xi + A_4\sin\beta\xi \\ &\quad + A_5\cos\gamma\xi + A_6\sin\gamma\xi \\ \Phi(\xi) &= B_1\cosh\alpha\xi + B_2\sinh\alpha\xi + B_3\cos\beta\xi + B_4\sin\beta\xi \\ &\quad + B_5\cos\gamma\xi + B_6\sin\gamma\xi \end{aligned} \tag{A3}$$

where

$$\alpha = [2(q/3)^{1/2}\cos(\varphi/3) - u/3]^{1/2}$$
$$\beta = \{2(q/3)^{1/2}\cos[(\pi-\varphi)/3] + u/3\}^{1/2}$$
$$\gamma = \{2(q/3)^{1/2}\cos[(\pi+\varphi)/3] + u/3\}^{1/2}$$

with

$$q = v + u^2/3$$
$$\varphi = \cos^{-1}\{(27uvw - 9uv - 2u^3)/[2(u^2+3v)^{3/2}]\}$$

and u, v and w are given in Eq. (A2). After an algebraic manipulation, it can be shown that coefficients $A_{1\text{–}6}$ and $B_{1\text{–}6}$ are related by

$$B_1 = (k_\alpha A_2 - m_\alpha A_1)/l, \qquad B_2 = (k_\alpha A_1 - m_\alpha A_2)/l$$
$$B_3 = (m_\beta A_3 + k_\beta A_4)/l, \qquad B_4 = (m_\beta A_4 - k_\beta A_3)/l \tag{A4}$$
$$B_5 = (m_\gamma A_5 + k_\gamma A_6)/l, \qquad B_6 = (m_\gamma A_6 - k_\gamma A_5)/l$$

where

$$m_\alpha = -l^3 S_y \omega^2 t_\alpha, \qquad k_\alpha = K\alpha^3 t_\alpha, \qquad m_\beta = l^3 S_y \omega^2 t_\beta$$
$$k_\beta = K\beta^3 t_\beta, \qquad m_\gamma = l^3 S_y \omega^2 t_\gamma, \qquad k_\gamma = K\gamma^3 t_\gamma$$

with

$$t_\alpha = \frac{EI\alpha^4 - l^4 m\omega^2}{K^2\alpha^6 - l^6 S_y^2 \omega^4}, \qquad t_\beta = \frac{EI\beta^4 - l^4 m\omega^2}{K^2\beta^6 + l^6 S_y^2 \omega^4}$$
$$t_\gamma = \frac{EI\gamma^4 - l^4 m\omega^2}{K^2\gamma^6 + l^6 S_y^2 \omega^4}$$

Note that rather than the one-to-one relation in Eq. 15 of [25], two coefficients in $A_{1\text{–}6}$ are now coupled with two coefficients in $B_{1\text{–}6}$.

Substituting Eq. (A4) into Eq. (A3) yields the dimensionless expression for the twisting angle:

$$\Phi(\xi) = [(k_\alpha \sinh\alpha\xi - m_\alpha \cosh\alpha\xi)A_1 + (k_\alpha \cosh\alpha\xi - m_\alpha \sinh\alpha\xi)A_2 + (m_\beta \cos\beta\xi - k_\beta \sin\beta\xi)A_3 + (m_\beta \sin\beta\xi - k_\beta \cos\beta\xi)A_4 + (m_\gamma \cos\gamma\xi - k_\gamma \sin\gamma\xi)A_5 + (m_\gamma \sin\gamma\xi - k_\gamma \cos\gamma\xi)A_6]/l \tag{A5}$$

At any cross section, the cross-sectional rotation, the bending moment, the shear force, and the torsional moment with the normalized coordinate ξ become

$$\Theta(\xi) = \frac{1}{l}\frac{dH(\xi)}{d\xi} = \frac{1}{l}[A_1\alpha\sinh\alpha\xi + A_2\alpha\cosh\alpha\xi - A_3\beta\sin\beta\xi + A_4\beta\cos\beta\xi - A_5\gamma\sin\gamma\xi + A_6\gamma\cos\gamma\xi] \tag{A6}$$

$$M(\xi) = \frac{EI}{l^2}\frac{d^2H(\xi)}{d\xi^2} - \frac{K}{l}\frac{d\Phi(\xi)}{d\xi} = \frac{EI}{l^2}[(r_\alpha \sinh\alpha\xi - n_\alpha \cosh\alpha\xi)A_1 + (r_\alpha \cosh\alpha\xi - n_\alpha \sinh\alpha\xi)A_2 + (n_\beta \cos\beta\xi + r_\beta \sin\beta\xi)A_3 + (n_\beta \sin\beta\xi - r_\beta \cos\beta\xi)A_4 + (n_\gamma \cos\gamma\xi + r_\gamma \sin\gamma\xi)A_5 + (n_\gamma \sin\gamma\xi - r_\gamma \cos\gamma\xi)A_6] \tag{A7}$$

$$S(\xi) = -\frac{1}{l}\frac{dM(\xi)}{d\xi} = \frac{EI}{l^3}[\alpha(n_\alpha \sinh\alpha\xi - r_\alpha \cosh\alpha\xi)A_1 + \alpha(n_\alpha \cosh\alpha\xi - r_\alpha \sinh\alpha\xi)A_2 + \beta(n_\beta \sin\beta\xi - r_\beta \cos\beta\xi)A_3 - \beta(n_\beta \cos\beta\xi + r_\beta \sin\beta\xi)A_4 + \gamma(n_\gamma \sin\gamma\xi - r_\gamma \cos\gamma\xi)A_5 - \gamma(n_\gamma \cos\gamma\xi + r_\gamma \sin\gamma\xi)A_6] \tag{A8}$$

$$T(\xi) = -\frac{K}{l^2}\frac{d^2H(\xi)}{d\xi^2} + \frac{GJ}{l^2}\frac{d\Phi(\xi)}{d\xi} = \frac{GJ}{l^2}[-(p_\alpha \cosh\alpha\xi + g_a \sinh\alpha\xi)A_1 - (p_\alpha \sinh\alpha\xi + g_a \cosh\alpha\xi)A_2 + (p_\beta \cos\beta\xi - g_\beta \sin\beta\xi)A_3 + (p_\beta \sin\beta\xi + g_\beta \cos\beta\xi)A_4 + (p_\gamma \cos\gamma\xi - g_\gamma \sin\gamma\xi)A_5 + (p_\gamma \sin\gamma\xi + g_\gamma \cos\gamma\xi)A_6] \tag{A9}$$

where

$$n_i = i(Kk_i - i\cdot EI)/EI, \qquad r_i = iKm_i/EI$$
$$p_i = i(iK - GJ\cdot k_i)/GJ, \qquad g_i = im_i, \quad \text{where } i = \alpha,\ \beta,\ \text{or } \gamma$$

Appendix B: Coefficients in Eqs. (15) to (20)

Coefficients a_{11} to d_{22} in Eqs. (15) and (18) can be determined to be

$$a_{11} = EI\left(\int_0^{l_c} f_1^{iv} f_1\,dy + \int_{l_c}^{l} f_2^{iv} f_2\,dy\right)$$
$$a_{12} = -K\left(\int_0^{l_c} g_1''' f_1\,dy + \int_{l_c}^{l} g_2''' f_2\,dy\right)$$
$$a_{21} = K\left(\int_0^{l_c} f_1''' g_1\,dy + \int_{l_c}^{l} f_2''' g_2\,dy\right)$$
$$a_{22} = -GJ\left(\int_0^{l_c} g_1'' g_1\,dy + \int_{l_c}^{l} g_2'' g_2\,dy\right)$$
$$b_{12} = L_1\left(\int_0^{l_c} g_1 f_1\,dy + \int_{l_c}^{l} g_2 f_2\,dy\right)$$
$$b_{22} = -M_1\left(\int_0^{l_c} g_1^2\,dy + \int_{l_c}^{l} g_2^2\,dy\right)$$
$$c_{11} = m\left(\int_0^{l_c} f_1^2\,dy + \int_{l_c}^{l} f_2^2\,dy\right)$$
$$c_{22} = I_y\left(\int_0^{l_c} g_1^2\,dy + \int_{l_c}^{l} g_2^2\,dy\right)$$
$$c_{12} = S_y\left(\int_0^{l_c} g_1 f_1\,dy + \int_{l_c}^{l} g_2 f_2\,dy\right) = c_{21}$$
$$d_{11} = L_1\left(\int_0^{l_c} f_1^2\,dy + \int_{l_c}^{l} f_2^2\,dy\right)$$
$$d_{12} = L_2\left(\int_0^{l_c} g_1 f_1\,dy + \int_{l_c}^{l} g_2 f_2\,dy\right)$$
$$d_{21} = -M_1\left(\int_0^{l_c} f_1 g_1\,dy + \int_{l_c}^{l} f_2 g_2\,dy\right)$$
$$d_{22} = -M_2\left(\int_0^{l_c} g_1^2\,dy + \int_{l_c}^{l} g_2^2\,dy\right)$$

Here, coefficients d_{11} to d_{22} are applicable to the quasi-steady aerodynamic model only; they need to be set to zero in deriving the corresponding coefficients for the steady aerodynamic model. From Eqs. (15) and (18), coefficients A_1 to F_1 in Eq. (16) and A_0 to E_0 in Eq. (17) can be determined to be

$$A_1 = c_{11}c_{22} - c_{12}c_{21}, \qquad B_1 = a_{11}c_{22} + a_{22}c_{11} - a_{21}c_{12} - a_{12}c_{21},$$
$$B_2 = c_{11}d_{22} + c_{22}d_{11} - c_{21}d_{12} - c_{12}d_{21}$$
$$C_1 = b_{22}c_{11} + d_{11}d_{22} - b_{12}c_{21} - d_{12}d_{21}$$
$$D_1 = a_{11}a_{22} - a_{12}a_{21}$$
$$D_2 = a_{11}d_{22} + a_{22}d_{11} - a_{21}d_{12} - a_{12}d_{21}$$
$$F_1 = a_{11}b_{22} - a_{21}b_{12}, \qquad F_2 = b_{22}d_{11} - b_{12}d_{21}$$

and

$$A_0 = A_1, \qquad B_0 = B_2 U, \qquad C_0 = B_1 + C_1 U^2$$
$$D_0 = D_2 U + F_2 U^3, \qquad E_0 = D_1 + F_1 U^2$$

Acknowledgment

The authors gratefully acknowledge financial support for this research by the Los Alamos National Laboratory under grant number 44238-001-0245.

References

[1] Sih, G. C., and Chen, E. P., *Mechanics of Fracture*, Vol. 6, Martinus–Nijhoff, Dordrecht, The Netherlands, 1981.

[2] Starnes, J. H., Jr., and Haftka, R. T., "Preliminary Design of Composite Wing Box Structures for Global Damage Tolerance," *A Collection of Technical Papers: AIAA/ASME/ASCE/AHS 21st Structures, Structural Dynamics and Materials Conference*, AIAA, New York, May 1980, pp. 529–538.

[3] Eastep, F. E., Venkayya, V. B., and Tishler, V. A., "Divergence Speed Degradation of Forward-Swept Wings with Damaged Composite Skin," *Journal of Aircraft*, Vol. 21, No. 11, 1984, pp. 921–923.

[4] Kosmatka, J. B., and Panza, J., "Aeroelastic Stability of the GA-ASI Predator Aircraft," AIAA's First Technical Conference and Workshop on Unmanned Aerospace Vehicles, Systems, Technologies, and Operations, Portsmouth, VA, AIAA Paper 2002-3470, May 2002.

[5] Chen, W.-H., and Lin, H.-C., "Flutter Analysis of Thin Cracked Panels Using the Finite Element Method," *AIAA Journal*, Vol. 23, No. 5, 1985, pp. 795–801.

[6] Kapania, R. K., and Castel, F., "A Simple Element for Aeroelastic Analysis of Undamaged and Damaged Wings," *AIAA Journal*, Vol. 28, No. 2, 1990, pp. 329–331.

[7] Strganac, T. W., and Kim, Y. I., "Aeroelastic Behavior of Composite Plates Subject to Damage Growth," *Journal of Aircraft*, Vol. 33, No. 1, 1996, pp. 68–73.

[8] Bauchau, O. A., Zhang, H. C., Loewy, R. G., and Atluri, S. N., "Nonlinear Aeroelastic Effects in Damaged Composite Aerospace Structures," AIAA Paper 97-0577, Jan. 1997.

[9] Kim, T., Atluri, S. N., and Loewy, R. G., "Modeling of Microcrack Damaged Composite Plates Under Bimodular Flutter Oscillations," *AIAA Journal*, Vol. 36, No. 4, 1998, pp. 598–606.

[10] Cesnik, C. E. S., Hodges, D. H., and Patil, M. J., "Aeroelastic Analysis of Composite Wings," *37th AIAA/ASME/ASCE/AHS/ASC Structures, Structural Dynamics, and Materials Conference*, AIAA, Washington, D.C., 1996, pp. 1113–1123.

[11] Bisplinghoff, R. L., Ashley, H., and Halfman, R. L., *Aeroelasticity*, Dover, New York, 1996.

[12] Fung, Y. C., *An Introduction to the Theory of Aeroelasticity*, Dover, New York, 1969.

[13] Stein, M., and Housner, J. G., "Flutter Analysis of Swept-Wing Subsonic Aircraft with Parameter Studies of Composite Wings," NASA TN D-7539, 1974.

[14] Weisshaar, T. A., "Aeroelastic Stability and Performance Characteristics of Aircraft with Advanced Composite Sweptforward Wing Structures," U.S. Air Force Flight Dynamics Laboratory Rept. TR-78-116, 1978.

[15] Weisshaar, T. A., "Aeroelastic Tailoring of Forward Swept Composite Wings," *Journal of Aircraft*, Vol. 18, No. 8, 1981, pp. 669–676.

[16] Lottati, I., "Flutter and Divergence Aeroelastic Characteristics for Composite Forward Swept Cantilevered Wing," *Journal of Aircraft*, Vol. 22, No. 11, 1985, pp. 1001–1007.

[17] Weisshaar, T. A., and Foist, B. L., "Vibration Tailoring of Advanced Composite Lifting Surfaces," *Journal of Aircraft*, Vol. 22, No. 2, 1985, pp. 141–147.

[18] Guo, S. J., Bannerjee, J. R., and Cheung, C. W., "The Effect of Laminate Lay-Up on the Flutter Speed of Composite Wings," *Proceedings of the Institute of Mechanical Engineers, Part G: Journal of Aerospace Engineering*, Vol. 217, No. 3, 2003, pp. 115–122.

[19] Rehfield, L. W., Atilgan, A. R., and Hodges, D. H., "Nonclassical Behavior of Thin-Walled Composite Beam with Closed Cross Sections," *Journal of the American Helicopter Society*, Vol. 35, No. 2, 1990, pp. 42–50.

[20] Chandra, R., Stemple, A. D., and Chopra, I., "Thin-Walled Composite Beams Under Bending, Torsional, and Extensional Loads," *Journal of Aircraft*, Vol. 27, No. 7, 1990, pp. 619–626.

[21] Smith, E. C., and Chopra, I., "Formulation and Evaluation of an Analytical Model for Composite Box-Beam," *Journal of the American Helicopter Society*, Vol. 36, No. 3, 1991, pp. 23–35.

[22] Dancila, D. S., and Armanios, E. A., "The Influence of Coupling on the Free Vibration of Anisotropic Thin-Walled Closed-Section Beams," *International Journal of Solids and Structures*, Vol. 35, No. 23, 1998, pp. 3108–3119.

[23] Librescu, L., and Song, O., "On the Static Aeroelastic Tailoring of Composite Aircraft Swept Wings Modeled as Thin-Walled Beam Structures," *Composites Engineering*, Vol. 2, No. 5–7, 1992, pp. 497–512.

[24] Qin, Z., Librescu, L., and Marzocca, P., "Aeroelasticity of Composite Aerovehicle Wings in Supersonic Flows," *Journal of Spacecraft and Rockets*, Vol. 40, No. 2, 2003, pp. 162–173.

[25] Wang, K., Inman, D. J., and Farrar, C. R., "Modeling and Analysis of a Cracked Composite Cantilever Beam Vibrating in Coupled Bending and Torsion," *Journal of Sound and Vibration*, Vol. 284, No. 1–2, 2005, pp. 23–49.

[26] Librescu, L., Meirovitch, L., and Song, O., "Refined Structural Modeling for Enhancing Vibrational and Aeroelastic Characteristics of Composite Aircraft Wings," *La Recherche Aérospatiale*, No. 1, 1996, pp. 23–35.

[27] Gern, F. H., and Librescu, L., "Aeroelastic Tailoring of Composite Wings Exhibiting Nonclassical Effects and Carrying External Stores," *Journal of Aircraft*, Vol. 37, No. 6, 2000, pp. 1097–1104.

[28] Dowell, E. H., Curtiss, H. C., Scanlan, R. H., and Sisto, F., *A Modern Course in Aeroelasticity*, Sijhoff and Noordhoff, Alphen aan den Rijn, The Netherlands, 1978.

[29] Lin, K-J., Lu, P-J., and Tarn, J-Q., "Flutter Analysis of Anisotropic Panels with Patched Cracks," *Journal of Aircraft*, Vol. 28, No. 12, 1991, pp. 899–907.

[30] Lin, K-J., Lu, P-J., and Tarn, J-Q., "Flutter Analysis of Cantilever Composite Plates in Subsonic Flow," *AIAA Journal*, Vol. 27, No. 8, 1989, pp. 1102–1109.

C. Pierre
Associate Editor